

# Beam-energy dependence of correlations between mean transverse momentum and anisotropic flow of charged particles in Au+Au collisions at RHIC

The STAR Collaboration

---

## Abstract

The correlation between the mean transverse momentum,  $[p_T]$ , and the squared anisotropic flow,  $v_n^2$ , on an event-by-event basis has been suggested to be influenced by the initial conditions in heavy-ion collisions. We present measurements of the variances and covariance of  $[p_T]$  and  $v_n^2$ , along with their dimensionless ratio, for Au+Au collisions at various beam energies:  $\sqrt{s_{NN}} = 14.6, 19.6, 27, 54.4$ , and  $200$  GeV. Our measurements reveal a distinct energy-dependent behavior in the variances and covariance. In addition, the dimensionless ratio displays a similar behavior across different beam energies. We compare our measurements with hydrodynamic models and similar measurements from Pb+Pb collisions at the Large Hadron Collider (LHC). These findings provide valuable insights into the beam energy dependence of the specific shear viscosity ( $\eta/s$ ) and initial-state effects, allowing for differentiating between different initial-state models.

---

Extensive experimental measurements of heavy-ion collisions at the Relativistic Heavy Ion Collider (RHIC) [1–4] and the Large Hadron Collider [5] demonstrate the formation of the Quark-Gluon Plasma (QGP), as predicted by Quantum Chromodynamics (QCD). Many of these investigations seek to characterize the QGP’s transport properties (e.g., the specific shear viscosity  $\eta/s$ ) [6, 7]. The anisotropic flow measurements, described by the azimuthal anisotropy of the particles emitted relative to collision symmetry planes, are important in many studies [8–13]. Specifically, anisotropic flow measurements reflect the viscous hydrodynamic response to the initial spatial distribution formed in the collision at early stages [14–22].

The anisotropic flow can be characterized by the Fourier expansion [23, 24] of the particle azimuthal angle ( $\phi$ ) distributions,

$$\frac{dN}{d\phi} \propto 1 + 2 \sum_{n=1}^{\infty} v_n \cos[n(\phi - \Psi_n)], \quad (1)$$

where  $\Psi_n$  is the  $n^{th}$ -order flow symmetry plane. The  $n^{th}$  complex anisotropic flow vector with  $v_n$  magnitude and  $\Psi_n$  direction is defined as  $V_n = v_n e^{in\Psi_n}$ . The first three flow coefficients are commonly termed the directed flow ( $v_1$ ), elliptic flow ( $v_2$ ), and triangular flow ( $v_3$ ). Anisotropic flow

measurements of the  $n^{th}$ -order flow harmonics [25–39], the correlation between different flow harmonics [40–42, 42–45], and flow fluctuations [36, 46–48] have led to a deeper understanding of the heavy-ion collision’s initial conditions [49, 50] and the properties of the matter created in heavy-ion collisions [51, 52].

Extensive comparisons between data and models across various collision energies and systems have indicated a low  $\eta/s$  for the QGP, yet significant uncertainties persist [8–10, 16, 18, 53]. These uncertainties primarily arise from the difficulty in constraining the initial conditions of the collision. As a result, current theoretical and experimental investigations have sought to identify observables that could offer additional insights and tighter constraints on the initial state of heavy-ion collisions. One recent proposal is to examine the correlation between the mean transverse momentum,  $[p_T]$ , and the squared anisotropic flow,  $v_n^2$ , on an event-by-event basis [54–59]. These correlations are quantified using the Pearson correlation coefficient;

$$\rho(v_n^2, [p_T]) = \frac{\text{Cov}(v_n^2, [p_T])}{\sqrt{\text{Var}(v_n^2)} \sqrt{\text{Var}([p_T])}}, \quad (2)$$

where,  $\text{Cov}(X, Y)$  and  $\text{Var}(X)$  represent the covariance of parameters  $X$  and  $Y$  and the variance of parameter  $X$  respectively.

The correlations between  $[p_T]$  and the  $v_n^2$  coefficients offer valuable insights into two key aspects: (i) the relationship between the size and eccentricities in the initial state, and (ii) the correlation between the strength of the hydrodynamic response and the flow coefficients. It is noteworthy that  $v_n^2$  ( $\text{Var}(v_n^2)$ ) is primarily influenced by eccentricities, while  $[p_T](\text{Var}([p_T]))$  is driven by the transverse size of the collision zone. Specifically, events with similar energy density but smaller transverse size tend to exhibit more radial expansion, leading to larger values of  $[p_T](\text{Var}([p_T]))$  [60]. Furthermore, several studies [59, 61–64] have highlighted the sensitivity of the  $\rho(v_n^2, [p_T])$  correlation to the initial-state nuclear deformation and the nuclear geometry of the colliding nuclei.

In this letter, we use the multiparticle cumulant method to study the  $\rho(v_2^2, [p_T])$  and its components ( $\text{Var}(v_2^2)$ ,  $\text{Var}([p_T])$  and  $\text{Cov}(v_2^2, [p_T])$ ) dependence on beam energy. These measurements are expected to provide a unique data set that is comprehensive and derived from a consistent analysis across the different beam energies presented.

The Au+Au data reported in this analysis were taken using a minimum-bias trigger, by the STAR detector [65] at  $\sqrt{s_{NN}} = 14.6, 19.6, 27.0, 54.4$ , and 200 GeV collected in the years 2019, 2019, 2018, 2017, and 2011, respectively. The collision vertices were reconstructed using tracks measured with charged-particle trajectories detected in the STAR Time Projection Chamber (TPC) in a 0.5 T magnetic field pointing along the beam direction (z-axis) [66]. Events were selected to have a vertex position about the nominal center of the TPC (in the beam direction) of  $\pm 30$  cm for Au+Au at  $\sqrt{s_{NN}} = 200$  GeV,  $\pm 40$  cm at  $\sqrt{s_{NN}} = 54.4$  and 27 GeV, and  $\pm 70$  cm at  $\sqrt{s_{NN}} = 19.6$  and 14.6 GeV and to be within a radius of  $r < 2$  cm with respect to the beam axis. Such cuts are used to minimize pileup effects and filter out interactions with the beam pipe.

In this work, the data sets are categorized into centrality classes based on the “reference multiplicity” in the STAR experiment. This reference multiplicity is typically calculated from the raw multiplicity of primary charged particles reconstructed in the TPC across the entire azimuthal range and within  $|\eta| < 0.5$ . The selection of  $|\eta| < 0.5$  is deliberate as it ensures a nearly uniform distribution of  $\eta$  in this range of the detector, and the tracks exhibit higher quality compared to those near the TPC edge. Centrality classes are estab-

lished by fitting the reference multiplicity distribution to that derived from Monte Carlo Glauber simulations [67, 68].

The  $\rho(v_n^2, [p_T])$  correlator is derived from covariance and variance (cf. Eq. 2) which involve both two- and multi-particle correlations. The two- and multi-particle correlations could be influenced by nonflow effects due to resonance decays, Bose-Einstein correlations, and the fragments of individual jets [69]. Since nonflow contributions mainly involve particles emitted within a localized region in pseudorapidity,  $\eta$ , they can be suppressed via sub-event cumulant methods [70–74]. In the sub-event cumulant methods, the correlated particles are taken from two or more sub-events that are separated in  $\eta$ . The efficiency of these methods to reduce nonflow effects has been quantified for many different two- and multi-particle correlators [22, 70, 71, 73–75].

In this work, charged particles with  $0.2 < pT < 2.0$  (GeV) is used. The traditional and two-subevent cumulant methods, which incorporate weights to account for acceptance and efficiency [70], are employed in this study to construct the  $v_n^2$  variance. Specifically, the  $\eta$  range of  $0.35 < |\eta| < 1.0$  is selected to measure the two-particle  $v_n\{2\}$  and the four-particle  $v_2\{4\}$  using the two-subevent and traditional cumulant methods, respectively. Two subevents, A and C are defined, where all tracks in sub-event A are required to be within  $-1.0 < \eta_A < -0.35$  and all tracks in sub-event C are required to be within  $0.35 < \eta_C < 1.0$ . The  $v_n^2$  dynamical variance is given as [76]:

$$\begin{aligned}\text{Var}(v_2^2)_{dyn} &= v_2\{2\}^4 - v_2\{4\}^4, \\ &= C_2^2\{2\} - C_2\{4\}, \\ \text{Var}(v_3^2)_{dyn} &= v_3\{2\}^4 = C_3^2\{2\}.\end{aligned}\quad (3)$$

The two-particle flow harmonics  $v_n\{2\}$  can be given as:

$$\begin{aligned}C_n\{2\} &= \langle\langle 2_n \rangle\rangle|_{AC} = \langle\langle e^{i n(\varphi_1^A - \varphi_2^C)} \rangle\rangle, \\ v_n\{2\} &= \sqrt{C_n\{2\}}\end{aligned}\quad (4)$$

where  $\varphi_{A(C)}$  is the azimuthal angle of particles in the region  $A(C)$  and  $\langle\langle 2_n \rangle\rangle$  is the two particle correlations of order  $n$ . In addition, the four-particle flow harmonic  $v_2\{4\}$  can be given as:

$$\begin{aligned}C_2\{4\} &= \langle\langle 4_2 \rangle\rangle - 2\langle\langle 2_2 \rangle\rangle^2, \\ &= \langle\langle e^{i 2(\varphi_1 + \varphi_2 - \varphi_3 - \varphi_4)} \rangle\rangle \\ &- 2 \langle\langle e^{i 2(\varphi_1 - \varphi_2)} \rangle\rangle \\ v_2\{4\} &= \sqrt[4]{-C_2\{4\}},\end{aligned}\quad (5)$$

where  $\langle\langle 4_2 \rangle\rangle$  is the four particle correlations of order 2.

The dynamical  $p_T$  correlations ( $C_k$ ) [55, 77, 78] in region  $B$  ( $|\eta_B| < 0.35$ ) are defined as:

$$C_k = \left\langle \frac{1}{N_{\text{pair}}} \sum_b \sum_{b' \neq b} (p_{T,b} - \langle [p_T] \rangle)(p_{T,b'} - \langle [p_T] \rangle) \right\rangle, \quad (6)$$

where  $\langle \rangle$  is an average over all events, and the two particles  $b$  and  $b'$  are required to be separated by an eta gap of 0.2. The event mean  $p_T$ ,  $[p_T]$ , is given as,

$$[p_T] = \sum_{i=1}^{M_B} p_{T,i} / M_B, \quad (7)$$

where  $M_B$  is the event multiplicity in sub-event  $B$ . The covariance between  $v_2^2$  and  $[p_T]$ ,  $\text{Cov}(v_2^2, [p_T])$ , is defined using the three-subevents method [74, 79] as,

$$\text{Cov}(v_n^2, [p_T]) = \langle \langle 2_n \rangle |_{AC} ([p_T] - \langle [p_T] \rangle)_B \rangle. \quad (8)$$

The resulting  $\rho(v_2^2, [p_T])$  correlator [54–59, 80], is obtained via Eqs. 3, 6 and 8:

$$\rho(v_n^2, [p_T]) = \frac{\text{Cov}(v_n^2, [p_T])}{\sqrt{\text{Var}(v_n^2)_{dyn}} C_k}. \quad (9)$$

The presented measurement's systematic uncertainties are evaluated from variations in the analysis cuts for event selection, track selection, and nonflow suppression. (i) The systematic errors due to the event selection were obtained by modifying the vertex selection criteria to require the vertex position to be in either the positive or negative half of the allowed region along the beam. (ii) Track selection was varied by (a) reducing the distance of the closest approach (DCA) between a track and the primary vertex from its nominal value of 3 cm to 2 cm and (b) increasing the number of TPC space points used from more than 15 points to more than 20 points. (iii) The pseudorapidity gap,  $\Delta\eta = \eta_1 - \eta_2$  for the track pairs, used to reduce the nonflow effects due to resonance decays, Bose-Einstein correlations, and the fragments of individual jets, was varied from  $\Delta\eta = 0.7$  to  $\Delta\eta = 0.9$ . The overall systematic uncertainty, assuming independent sources, was taken to be the quadrature sum of the uncertainties resulting from the respective cut variations. Depending on beam energy, they range from 5% to 9% from central to peripheral collisions. The  $\Delta\eta$

variation is the dominant systematic uncertainty source.

The comprehensive beam energy measurements reported in this paper help theoretical models constrain their initial conditions and better estimate how  $\eta/s$  varies with baryon chemical potential and temperature. Hence, it is instructive to compare our measurements to available theoretical predictions. In this work, our measurements at  $\sqrt{s_{NN}} = 200$  GeV are compared to two theoretical models: (i) The IP-Glasma+(3+1)D MUSIC+UrQMD model [56, 81], which utilizes an initial state generated from the IP-Glasma framework, followed by the MUSIC viscous hydrodynamic model with  $\eta/s$  of 0.12, and the UrQMD afterburner. (ii) The Trento+Hydro model [82], which employs initial conditions from the T<sub>R</sub>ENTO model with a viscous hydrodynamic model with  $\eta/s$  of 0.05. In both models, the  $\eta/s$  value selection was chosen to reproduce the experimental measurements of the anisotropic flow and particle spectra.

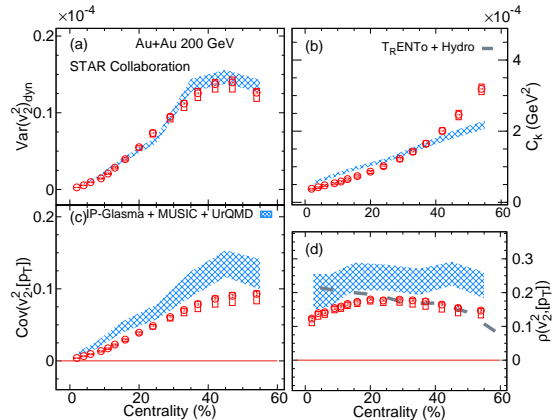


Figure 1: Comparison of the centrality dependence of (a)  $\text{Var}(v_2^2)_{dyn}$ , (b)  $C_k$ , (c)  $\text{Cov}(v_2^2, [p_T])$ , and (d)  $\rho(v_2^2, [p_T])$ , for Au+Au collisions at  $\sqrt{s_{NN}} = 200$  GeV. Measurements are compared to theoretical calculations represented as hatched bands [81] and dashed curve [82].

Figure 1 shows the centrality dependence of (a)  $\text{Var}(v_2^2)_{dyn}$ , (b)  $C_k$ , (c)  $\text{Cov}(v_2^2, [p_T])$ , and (d)  $\rho(v_2^2, [p_T])$  for Au+Au at  $\sqrt{s_{NN}} = 200$  GeV. The shaded bands in panels (a)–(d) and the dashed curve in panel (d) give the viscous hydrodynamic predictions by the IP-Glasma+MUSIC+UrQMD model [81] and the hydrodynamic model with Trento initial conditions [82]. Although, the hydrodynamic model calculations [81] show good agreement with the  $\text{Var}(v_2^2)_{dyn}$  and  $\sqrt{C_k}$ , it overpredicts

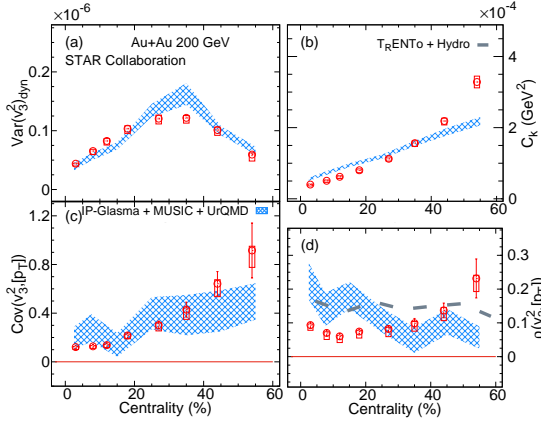


Figure 2: Comparison of the centrality dependence of (a)  $\text{Var}(v_3^2)_{\text{dyn}}$ , (b)  $C_k$ , (c)  $\text{Cov}(v_3^2, [p_T])$ , and (d)  $\rho(v_3^2, [p_T])$ , for Au+Au collisions at  $\sqrt{s_{NN}} = 200$  GeV. Measurements are compared to theoretical calculations represented as hatched bands [81] and dashed curve [82].

the  $\text{Cov}(v_2^2, [p_T])$  and  $\rho(v_2^2, [p_T])$  measurements. In addition, the two theoretical calculations show a different magnitude for the  $\rho(v_2^2, [p_T])$ .

Figure 2 shows the centrality dependence of the  $\text{Var}(v_3^2)_{\text{dyn}}$  (a),  $C_k$  (b),  $\text{Cov}(v_3^2, [p_T])$  (c), and  $\rho(v_3^2, [p_T])$  (d) for Au+Au at  $\sqrt{s_{NN}} = 200$  GeV. The shaded bands in panels (a)-(d) and the dashed curve in panel (d) show the viscous hydrodynamic calculations of the presented quantities [81, 82]. The theoretical calculations [81] show reasonable agreement with the  $\text{Var}(v_3^2)_{\text{dyn}}$ ,  $C_k$ , and the  $\text{Cov}(v_3^2, [p_T])$ , however, they over predicts the  $\rho(v_3^2, [p_T])$  measurements in central collisions. Data-model comparisons of both  $\rho(v_2^2, [p_T])$  and  $\rho(v_3^2, [p_T])$ , Figs 1 and 2, can be used to differentiate between different theoretical models.

Figure 3 shows the centrality dependence of  $\text{Var}(v_2^2)_{\text{dyn}}$  (a),  $C_k$  (b),  $\text{Cov}(v_2^2, [p_T])$  (c), and  $\rho(v_2^2, [p_T])$  (d) at five different beam energies. The measurements in panels (a)-(c) show that the magnitudes of  $\text{Var}(v_2^2)_{\text{dyn}}$ ,  $\sqrt{C_k}$ , and  $\text{Cov}(v_2^2, [p_T])$  decreases with beam energy over the full centrality range. Such behavior would reflect the beam energy dependence of the final state effect, given that the initial state is not a strong function in beam energy [84–87]. In contrast, the values for  $\rho(v_2^2, [p_T])$  panel (d) show weak beam energy dependence. The  $\rho(v_2^2, [p_T])$  are compared to published LHC measurements at 5.02 TeV [83]. The difference between RHIC and LHC measurements could arise from the  $[p_T]$  difference between the two measurements.

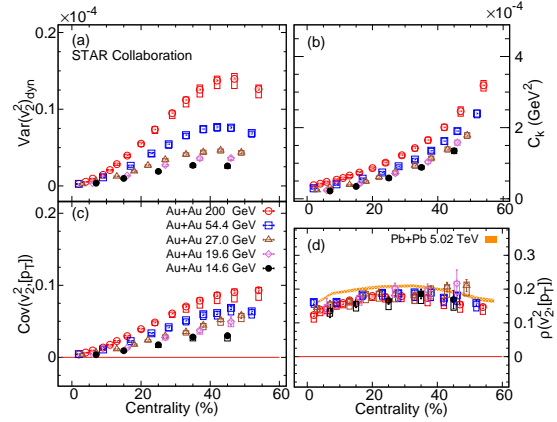


Figure 3: Comparison of the centrality dependence of (a)  $\text{Var}(v_2^2)_{\text{dyn}}$ , (b)  $C_k$ , (c)  $\text{Cov}(v_2^2, [p_T])$ , and (d)  $\rho(v_2^2, [p_T])$ , for Au+Au collisions at  $\sqrt{s_{NN}} = 200, 54.4, 27, 19.6$ , and  $14.6$  GeV. The curve represents the LHC measurements [83].

The beam energy measurements and their comparisons to the LHC measurements [83] indicate that the beam energy dependence of  $\text{Var}(v_2^2)_{\text{dyn}}$  and  $\text{Cov}(v_2^2, [p_T])$  could potentially provide important constraints for  $\eta/s$ . In contrast, the measurements for  $\rho(v_2^2, [p_T])$  provide complimentary constraints for the initial-state eccentricity and its fluctuations.

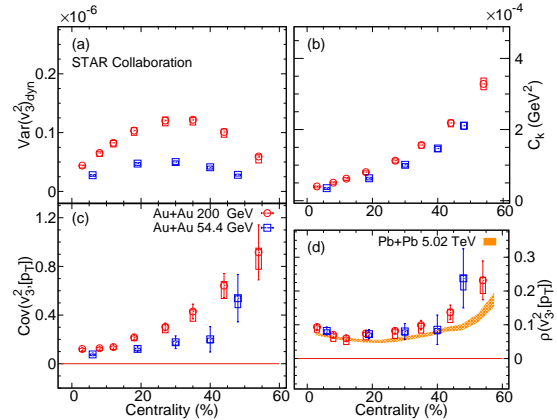


Figure 4: The centrality dependence of the  $\text{Var}(v_3^2)_{\text{dyn}}$  (a),  $C_k$  (b),  $\text{Cov}(v_3^2, [p_T])$  (c), and  $\rho(v_3^2, [p_T])$  (d), for Au+Au collisions at  $\sqrt{s_{NN}} = 200$  and  $54.4$  GeV. The curve represents the LHC measurements [83].

The centrality and beam-energy dependence of  $\text{Var}(v_3^2)_{\text{dyn}}$  (a),  $C_k$  (b),  $\text{Cov}(v_3^2, [p_T])$  (c), and  $\rho(v_3^2, [p_T])$  (d) are presented in Fig. 4. Our presented measurements in Fig. 4 are shown at high energies (i.e.,  $\sqrt{s_{NN}} = 200$  and  $54.4$  GeV) due to sta-

tistical limitations at lower energies. The  $\rho(v_3^2, [p_T])$  panel (d) are compared to similar LHC measurements [83]. Similar to the measurements in Fig. 3, the magnitudes of  $\text{Var}(v_3^2)_{\text{dyn}}$  and  $\text{Cov}(v_3^2, [p_T])$  decrease with beam energy. In contrast, the  $\rho(v_3^2, [p_T])$  panel (d) shows weak, if any, beam energy dependence. The  $\rho(v_3^2, [p_T])$  are also compared to similar LHC measurements [83]. Our measurements indicate that the beam energy dependence of  $\text{Var}(v_3^2)_{\text{dyn}}$  and  $\text{Cov}(v_3^2, [p_T])$  could potentially provide valuable constraints for extracting  $\eta/s$ . Additionally,  $\rho(v_3^2, [p_T])$  offers complementary constraints on the initial-state eccentricities and their correlations.

In summary, we have presented new  $p_T$ -integrated measurements of the charge-inclusive,  $C_k$ ,  $\text{Var}(v_n^2)_{\text{dyn}}$ ,  $\text{Cov}(v_n^2, [p_T])$  and  $\rho(v_n^2, [p_T])$  for Au+Au collisions at  $\sqrt{s_{NN}} = 200, 54.4, 27, 19.6$  and  $14.6$  GeV. Our measurements are compared with similar LHC measurements for Pb+Pb collisions at  $\sqrt{s_{NN}} = 5.02$  TeV. The measurements show characteristic patterns for the beam energy dependence of the variances of  $[p_T]$  and  $v_n^2$ , and the covariance  $\text{Cov}(v_2^2, [p_T])$ , consistent with the change of the final state effect with decreasing the beam energy. By contrast, the correlation coefficient  $\rho(v_n^2, [p_T])$  is shown to have weak dependent on beam energy. These measurements suggest that the beam energy dependence of  $C_k$ ,  $\text{Var}(v_n^2)_{\text{dyn}}$ ,  $\text{Cov}(v_n^2, [p_T])$  and  $\rho(v_n^2, [p_T])$ , could aid in a precision extraction of the temperature and baryon-chemical-potential dependence of  $\eta/s$ .

## Acknowledgments

We thank the RHIC Operations Group and RCF at BNL, the NERSC Center at LBNL, and the Open Science Grid consortium for providing resources and support. This work was supported in part by the Office of Nuclear Physics within the U.S. DOE Office of Science, the U.S. National Science Foundation, National Natural Science Foundation of China, Chinese Academy of Science, the Ministry of Science and Technology of China and the Chinese Ministry of Education, the Higher Education Sprout Project by Ministry of Education at NCKU, the National Research Foundation of Korea, Czech Science Foundation and Ministry of Education, Youth and Sports of the Czech Republic, Hungarian National Research, Development and Innovation Office, New National Excellency Programme of the Hungarian Ministry of

Human Capacities, Department of Atomic Energy and Department of Science and Technology of the Government of India, the National Science Centre and WUT ID-UB of Poland, the Ministry of Science, Education and Sports of the Republic of Croatia, German Bundesministerium für Bildung, Wissenschaft, Forschung and Technologie (BMBF), Helmholtz Association, Ministry of Education, Culture, Sports, Science, and Technology (MEXT), Japan Society for the Promotion of Science (JSPS) and Agencia Nacional de Investigación y Desarrollo (ANID) of Chile.

## References

- [1] J. Adams, et al., Experimental and theoretical challenges in the search for the quark gluon plasma: The STAR Collaboration's critical assessment of the evidence from RHIC collisions, *Nucl. Phys. A* 757 (2005) 102–183. [arXiv:nucl-ex/0501009](https://arxiv.org/abs/nucl-ex/0501009), doi:10.1016/j.nuclphysa.2005.03.085.
- [2] K. Adcox, et al., Formation of dense partonic matter in relativistic nucleus-nucleus collisions at RHIC: Experimental evaluation by the PHENIX collaboration, *Nucl. Phys. A* 757 (2005) 184–283. [arXiv:nucl-ex/0410003](https://arxiv.org/abs/nucl-ex/0410003), doi:10.1016/j.nuclphysa.2005.03.086.
- [3] I. Arsene, et al., Quark gluon plasma and color glass condensate at RHIC? The Perspective from the BRAHMS experiment, *Nucl. Phys. A* 757 (2005) 1–27. [arXiv:nucl-ex/0410020](https://arxiv.org/abs/nucl-ex/0410020), doi:10.1016/j.nuclphysa.2005.02.130.
- [4] B. B. Back, et al., The PHOBOS perspective on discoveries at RHIC, *Nucl. Phys. A* 757 (2005) 28–101. [arXiv:nucl-ex/0410022](https://arxiv.org/abs/nucl-ex/0410022), doi:10.1016/j.nuclphysa.2005.03.084.
- [5] B. Muller, J. Schukraft, B. Wyslouch, First Results from Pb+Pb collisions at the LHC, *Ann. Rev. Nucl. Part. Sci.* 62 (2012) 361–386. [arXiv:1202.3233](https://arxiv.org/abs/1202.3233), doi:10.1146/annurev-nucl-102711-094910.
- [6] E. V. Shuryak, Quark-Gluon Plasma and Hadronic Production of Leptons, Photons and Psions, *Sov. J. Nucl. Phys.* 28 (1978) 408. doi:10.1016/0370-2693(78)90370-2.
- [7] E. V. Shuryak, Quantum Chromodynamics and the Theory of Superdense Matter, *Phys. Rept.* 61 (1980) 71–158. doi:10.1016/0370-1573(80)90105-2.
- [8] E. Shuryak, Why does the quark gluon plasma at RHIC behave as a nearly ideal fluid?, *Prog. Part. Nucl. Phys.* 53 (2004) 273–303. [arXiv:hep-ph/0312227](https://arxiv.org/abs/hep-ph/0312227), doi:10.1016/j.ppnp.2004.02.025.
- [9] M. Luzum, P. Romatschke, Conformal Relativistic Viscous Hydrodynamics: Applications to RHIC results at  $\sqrt{s_{NN}} = 200$ -GeV, *Phys. Rev. C* 78 (2008) 034915. [arXiv:0804.4015](https://arxiv.org/abs/0804.4015), doi:10.1103/PhysRevC.78.034915, 10.1103/PhysRevC.79.039903.
- [10] P. Bozek, Bulk and shear viscosities of matter created in relativistic heavy-ion collisions, *Phys. Rev. C* 81 (2010) 034909. [arXiv:0911.2397](https://arxiv.org/abs/0911.2397), doi:10.1103/PhysRevC.81.034909.
- [11] P. Danielewicz, R. A. Lacey, P. Gossiaux, C. Pinkenburg, P. Chung, J. Alexander, R. McGrath, Disappearance of elliptic flow: a new probe for

- the nuclear equation of state, Phys. Rev. Lett. 81 (1998) 2438–2441. [arXiv:nucl-th/9803047](#), doi:[10.1103/PhysRevLett.81.2438](#).
- [12] U. W. Heinz, P. F. Kolb, Early thermalization at RHIC, Nucl. Phys. A702 (2002) 269–280. [arXiv:hep-ph/0111075](#), doi:[10.1016/S0375-9474\(02\)00714-5](#).
- [13] T. Hirano, U. W. Heinz, D. Kharzeev, R. Lacey, Y. Nara, Hadronic dissipative effects on elliptic flow in ultrarelativistic heavy-ion collisions, Phys.Lett. B636 (2006) 299–304. [arXiv:nucl-th/0511046](#), doi:[10.1016/j.physletb.2006.03.060](#).
- [14] P. Huovinen, P. F. Kolb, U. W. Heinz, P. V. Ruuskanen, S. A. Voloshin, Radial and elliptic flow at rhic: Further predictions, Phys. Lett. B503 (2001) 58–64.
- [15] T. Hirano, K. Tsuda, Collective flow and two pion correlations from a relativistic hydrodynamic model with early chemical freeze out, Phys. Rev. C66 (2002) 054905. [arXiv:nucl-th/0205043](#), doi:[10.1103/PhysRevC.66.054905](#).
- [16] P. Romatschke, U. Romatschke, Viscosity Information from Relativistic Nuclear Collisions: How Perfect is the Fluid Observed at RHIC?, Phys.Rev.Lett. 99 (2007) 172301. [arXiv:0706.1522](#), doi:[10.1103/PhysRevLett.99.172301](#).
- [17] M. Luzum, Flow fluctuations and long-range correlations: elliptic flow and beyond, J. Phys. G38 (2011) 124026. [arXiv:1107.0592](#), doi:[10.1088/0954-3899/38/12/124026](#).
- [18] H. Song, S. A. Bass, U. Heinz, T. Hirano, C. Shen, 200 A GeV Au+Au collisions serve a nearly perfect quark-gluon liquid, Phys. Rev. Lett. 106 (2011) 192301, [Erratum: Phys. Rev. Lett.109,139904(2012)]. [arXiv:1011.2783](#), doi:[10.1103/PhysRevLett.106.192301](#), [10.1103/PhysRevLett.109d4599041103/PhysRevC.109.024906](#).
- [19] J. Qian, U. W. Heinz, J. Liu, Mode-coupling effects in anisotropic flow in heavy-ion collisions, Phys. Rev. C93 (6) (2016) 064901. [arXiv:1602.02813](#), doi:[10.1103/PhysRevC.93.064901](#).
- [20] B. Schenke, S. Jeon, C. Gale, Anisotropic flow in  $\sqrt{s} = 2.76$  TeV Pb+Pb collisions at the LHC, Phys.Lett. B702 (2011) 59–63. [arXiv:1102.0575](#), doi:[10.1016/j.physletb.2011.06.065](#).
- [21] N. Magdy, X. Sun, Z. Ye, O. Evdokimov, R. Lacey, Investigation of the Elliptic Flow Fluctuations of the Identified Particles Using the a Multi-Phase Transport Model, Universe 6 (9) (2020) 146. [arXiv:2009.02734](#), doi:[10.3390/universe6090146](#).
- [22] N. Magdy, Characterizing initial- and final-state effects of relativistic nuclear collisions, Phys. Rev. C 107 (2) (2023) 024905. [arXiv:2210.14091](#), doi:[10.1103/PhysRevC.107.024905](#).
- [23] S. Voloshin, Y. Zhang, Flow study in relativistic nuclear collisions by Fourier expansion of Azimuthal particle distributions, Z. Phys. C 70 (1996) 665–672. [arXiv:hep-ph/9407282](#), doi:[10.1007/s002880050141](#).
- [24] A. M. Poskanzer, S. A. Voloshin, Methods for analyzing anisotropic flow in relativistic nuclear collisions, Phys. Rev. C58 (1998) 1671–1678. [arXiv:nucl-ex/9805001](#), doi:[10.1103/PhysRevC.58.1671](#).
- [25] B. Alver, et al., System size, energy, pseudorapidity, and centrality dependence of elliptic flow, Phys. Rev. Lett. 98 (2007) 242302. [arXiv:nucl-ex/0610037](#), doi:[10.1103/PhysRevLett.98.242302](#).
- [26] C. Adler, et al., Elliptic flow from two and four particle correlations in Au+Au collisions at  $\sqrt{s_{NN}} = 130$ -GeV, Phys. Rev. C 66 (2002) 034904. doi:[10.1103/PhysRevC.66.034904](#).
- [27] J. Adams, et al., Azimuthal anisotropy at RHIC: The First and fourth harmonics, Phys. Rev. Lett. 92 (2004) 062301, [Erratum: Phys.Rev.Lett. 127, 069901 (2021)]. doi:[10.1103/PhysRevLett.127.069901](#).
- [28] A. Adare, et al., Measurement of two-particle correlations with respect to second- and third-order event planes in Au+Au collisions at  $\sqrt{s_{NN}} = 200$  GeV, Phys. Rev. C 99 (5) (2019) 054903. [arXiv:1803.01749](#), doi:[10.1103/PhysRevC.99.054903](#).
- [29] K. Aamodt, et al., Higher harmonic anisotropic flow measurements of charged particles in Pb-Pb collisions at  $\sqrt{s_{NN}}=2.76$  TeV, Phys. Rev. Lett. 107 (2011) 032301. doi:[10.1103/PhysRevLett.107.032301](#).
- [30] M. Aaboud, et al., Measurement of the azimuthal anisotropy of charged particles produced in  $\sqrt{s_{NN}} = 5.02$  TeV Pb+Pb collisions with the ATLAS detector, Eur. Phys. J. C 78 (12) (2018) 997. doi:[10.1140/epjc/s10052-018-6468-7](#).
- [31] S. Chatrchyan, et al., Azimuthal anisotropy of charged particles at high transverse momenta in PbPb collisions at  $\sqrt{s_{NN}} = 2.76$  TeV, Phys. Rev. Lett. 109 (2012) 022301. doi:[10.1103/PhysRevLett.109.022301](#).
- [32] S. Chatrchyan, et al., Measurement of the elliptic anisotropy of charged particles produced in PbPb collisions at  $\sqrt{s_{NN}}=2.76$  TeV, Phys. Rev. C 87 (1) (2013) 014902. [arXiv:1204.1409](#), doi:[10.1103/PhysRevC.87.014902](#).
- [33] N. Magdy, Characterizing the initial- and final-state effects in isobaric collisions at energies available at the BNL Relativistic Heavy Ion Collider, Phys. Rev. C 109 (2) (2024) 024906. [arXiv:2401.04083](#), doi:[10.1103/PhysRevC.109.024906](#).
- [34] N. Magdy, Beam-energy dependence of the azimuthal anisotropic flow from RHIC (2019). [arXiv:1909.09640](#).
- [35] J. Adam, et al., Azimuthal Harmonics in Small and Large Collision Systems at RHIC Top Energies, Phys. Rev. Lett. 122 (17) (2019) 172301. [arXiv:1901.08155](#), doi:[10.1103/PhysRevLett.122.172301](#).
- [36] N. Magdy, Collision system and beam energy dependence of anisotropic flow fluctuations, Nucl. Phys. A982 (2019) 255–258. [arXiv:1807.07638](#), doi:[10.1016/j.nuclphysa.2018.09.027](#).
- [37] N. Magdy, Beam Energy Dependence of the Linear and Mode-Coupled Flow Harmonics Using the a Multi-Phase Transport Model, Universe 9 (2) (2023) 107. [arXiv:2302.10373](#), doi:[10.3390/universe9020107](#).
- [38] L. Adamczyk, et al., Azimuthal anisotropy in Cu+Au collisions at  $\sqrt{s_{NN}} = 200$  GeV, Phys. Rev. C98 (1) (2018) 014915. [arXiv:1712.01332](#), doi:[10.1103/PhysRevC.98.014915](#).
- [39] N. Magdy, Viscous Damping of Anisotropic Flow in 7.7 – 200 GeV Au+Au Collisions, J. Phys. Conf. Ser. 779 (1) (2017) 012060. doi:[10.1088/1742-6596/779/1/012060](#).
- [40] J. Adam, et al., Correlation Measurements Between Flow Harmonics in Au+Au Collisions at RHIC, Phys. Lett. B783 (2018) 459–465. [arXiv:1803.03876](#), doi:[10.1016/j.physletb.2018.05.076](#).
- [41] J. Adam, et al., Correlated event-by-event fluctuations of flow harmonics in Pb-Pb collisions at  $\sqrt{s_{NN}} = 2.76$  TeV, Phys. Rev. Lett. 117 (2016) 182301. [arXiv:1604.07663](#),

- [doi:10.1103/PhysRevLett.117.182301](https://doi.org/10.1103/PhysRevLett.117.182301).
- [42] G. Aad, et al., Measurement of the correlation between flow harmonics of different order in lead-lead collisions at  $\sqrt{s_{NN}}=2.76$  TeV with the ATLAS detector, Phys. Rev. C92 (3) (2015) 034903. [arXiv:1504.01289](https://arxiv.org/abs/1504.01289), doi:[10.1103/PhysRevC.92.034903](https://doi.org/10.1103/PhysRevC.92.034903).
- [43] Z. Qiu, U. W. Heinz, Event-by-event shape and flow fluctuations of relativistic heavy-ion collision fireballs, Phys. Rev. C84 (2011) 024911. [arXiv:1104.0650](https://arxiv.org/abs/1104.0650), doi:[10.1103/PhysRevC.84.024911](https://doi.org/10.1103/PhysRevC.84.024911).
- [44] A. Adare, et al., Measurements of Higher-Order Flow Harmonics in Au+Au Collisions at  $\sqrt{s_{NN}} = 200$  GeV, Phys. Rev. Lett. 107 (2011) 252301. [arXiv:1105.3928](https://arxiv.org/abs/1105.3928), doi:[10.1103/PhysRevLett.107.252301](https://doi.org/10.1103/PhysRevLett.107.252301).
- [45] G. Aad, et al., Measurement of event-plane correlations in  $\sqrt{s_{NN}} = 2.76$  TeV lead-lead collisions with the ATLAS detector, Phys. Rev. C90 (2) (2014) 024905. [arXiv:1403.0489](https://arxiv.org/abs/1403.0489), doi:[10.1103/PhysRevC.90.024905](https://doi.org/10.1103/PhysRevC.90.024905).
- [46] B. Alver, et al., Importance of correlations and fluctuations on the initial source eccentricity in high-energy nucleus-nucleus collisions, Phys. Rev. C77 (2008) 014906. [arXiv:0711.3724](https://arxiv.org/abs/0711.3724), doi:[10.1103/PhysRevC.77.014906](https://doi.org/10.1103/PhysRevC.77.014906).
- [47] B. Alver, et al., Non-flow correlations and elliptic flow fluctuations in gold-gold collisions at  $\sqrt{s_{NN}} = 200$  GeV, Phys. Rev. C81 (2010) 034915. [arXiv:1002.0534](https://arxiv.org/abs/1002.0534), doi:[10.1103/PhysRevC.81.034915](https://doi.org/10.1103/PhysRevC.81.034915).
- [48] J.-Y. Ollitrault, A. M. Poskanzer, S. A. Voloshin, Effect of flow fluctuations and nonflow on elliptic flow methods, Phys. Rev. C80 (2009) 014904. [arXiv:0904.2315](https://arxiv.org/abs/0904.2315), doi:[10.1103/PhysRevC.80.014904](https://doi.org/10.1103/PhysRevC.80.014904).
- [49] E. Retinskaya, M. Luzum, J.-Y. Ollitrault, Constraining models of initial conditions with elliptic and triangular flow data, Phys. Rev. C 89 (1) (2014) 014902. [arXiv:1311.5339](https://arxiv.org/abs/1311.5339), doi:[10.1103/PhysRevC.89.014902](https://doi.org/10.1103/PhysRevC.89.014902).
- [50] J. S. Moreland, J. E. Bernhard, S. A. Bass, Alternative ansatz to wounded nucleon and binary collision scaling in high-energy nuclear collisions, Phys. Rev. C 92 (1) (2015) 011901. [arXiv:1412.4708](https://arxiv.org/abs/1412.4708), doi:[10.1103/PhysRevC.92.011901](https://doi.org/10.1103/PhysRevC.92.011901).
- [51] D. Teaney, The Effects of viscosity on spectra, elliptic flow, and HBT radii, Phys. Rev. C68 (2003) 034913. [arXiv:nucl-th/0301099](https://arxiv.org/abs/hep-th/0301099), doi:[10.1103/PhysRevC.68.034913](https://doi.org/10.1103/PhysRevC.68.034913).
- [52] H. Song, S. A. Bass, U. Heinz, Elliptic flow in 200 A GeV Au+Au collisions and 2.76 A TeV Pb+Pb collisions: insights from viscous hydrodynamics + hadron cascade hybrid model, Phys. Rev. C83 (2011) 054912. [arXiv:1103.2380](https://arxiv.org/abs/1103.2380), doi:[10.1103/PhysRevC.83.054912](https://doi.org/10.1103/PhysRevC.83.054912), [10.1103/PhysRevC.87.019902](https://doi.org/10.1103/PhysRevC.87.019902).
- [53] C. Shen, U. Heinz, P. Huovinen, H. Song, Radial and elliptic flow in Pb+Pb collisions at the Large Hadron Collider from viscous hydrodynamic, Phys. Rev. C 84 (2011) 044903. [arXiv:1105.3226](https://arxiv.org/abs/1105.3226), doi:[10.1103/PhysRevC.84.044903](https://doi.org/10.1103/PhysRevC.84.044903).
- [54] G. Giacalone, B. Schenke, C. Shen, Observable signatures of initial state momentum anisotropies in nuclear collisions, Phys. Rev. Lett. 125 (19) (2020) 192301. [arXiv:2006.15721](https://arxiv.org/abs/2006.15721), doi:[10.1103/PhysRevLett.125.192301](https://doi.org/10.1103/PhysRevLett.125.192301).
- [55] P. Bozek, Transverse-momentum-flow correlations in relativistic heavy-ion collisions, Phys. Rev. C 93 (4) (2016) 044908. [arXiv:1601.04513](https://arxiv.org/abs/1601.04513), doi:[10.1103/PhysRevC.93.044908](https://doi.org/10.1103/PhysRevC.93.044908).
- [56] B. Schenke, C. Shen, D. Teaney, Transverse momentum fluctuations and their correlation with elliptic flow in nuclear collision, Phys. Rev. C 102 (3) (2020) 034905. [arXiv:2004.00690](https://arxiv.org/abs/2004.00690), doi:[10.1103/PhysRevC.102.034905](https://doi.org/10.1103/PhysRevC.102.034905).
- [57] G. Giacalone, F. G. Gardim, J. Noronha-Hostler, J.-Y. Ollitrault, Correlation between mean transverse momentum and anisotropic flow in heavy-ion collisions, Phys. Rev. C 103 (2) (2021) 024909. [arXiv:2004.01765](https://arxiv.org/abs/2004.01765), doi:[10.1103/PhysRevC.103.024909](https://doi.org/10.1103/PhysRevC.103.024909).
- [58] S. H. Lim, J. L. Nagle, Exploring Origins for Correlations between Flow Harmonics and Transverse Momentum in Small Collision Systems (Unambiguous Ambiguity) (3 2021). [arXiv:2103.01348](https://arxiv.org/abs/2103.01348).
- [59] Measurement of flow and transverse momentum correlations in Pb+Pb collisions at  $\sqrt{s_{NN}} = 5.02$  TeV and Xe+Xe collisions at  $\sqrt{s_{NN}} = 5.44$  TeV with the ATLAS detector (1 2021).
- [60] P. Bozek, W. Broniowski, Transverse-momentum fluctuations in relativistic heavy-ion collisions from event-by-event viscous hydrodynamics, Phys. Rev. C 85 (2012) 044910. [arXiv:1203.1810](https://arxiv.org/abs/1203.1810), doi:[10.1103/PhysRevC.85.044910](https://doi.org/10.1103/PhysRevC.85.044910).
- [61] G. Giacalone, Observing the deformation of nuclei with relativistic nuclear collisions, Phys. Rev. Lett. 124 (20) (2020) 202301. [arXiv:1910.04673](https://arxiv.org/abs/1910.04673), doi:[10.1103/PhysRevLett.124.202301](https://doi.org/10.1103/PhysRevLett.124.202301).
- [62] G. Giacalone, Constraining the quadrupole deformation of atomic nuclei with relativistic nuclear collisions, Phys. Rev. C 102 (2) (2020) 024901. [arXiv:2004.14463](https://arxiv.org/abs/2004.14463), doi:[10.1103/PhysRevC.102.024901](https://doi.org/10.1103/PhysRevC.102.024901).
- [63] N. Magdy, Impact of nuclear deformation on collective flow observables in relativistic U+U collisions, Eur. Phys. J. A 59 (3) (2023) 64. [arXiv:2206.05332](https://arxiv.org/abs/2206.05332), doi:[10.1140/epja/s10050-023-00982-0](https://doi.org/10.1140/epja/s10050-023-00982-0).
- [64] Imaging Shapes of Atomic Nuclei in High-Energy Nuclear Collisions (1 2024). [arXiv:2401.06625](https://arxiv.org/abs/2401.06625).
- [65] M. E. Beddo, et al., STAR: Conceptual design report for the Solenoidal Tracker at RHIC (6 1992).
- [66] M. Anderson, et al., The Star time projection chamber: A Unique tool for studying high multiplicity events at RHIC, Nucl. Instrum. Meth. A499 (2003) 659–678. [arXiv:nucl-ex/0301015](https://arxiv.org/abs/nucl-ex/0301015), doi:[10.1016/S0168-9002\(02\)01964-2](https://doi.org/10.1016/S0168-9002(02)01964-2).
- [67] L. Adamczyk, et al., Inclusive charged hadron elliptic flow in Au + Au collisions at  $\sqrt{s_{NN}} = 7.7 - 39$  GeV, Phys. Rev. C 86 (2012) 054908. [doi:10.1103/PhysRevC.86.054908](https://arxiv.org/abs/10.1103/PhysRevC.86.054908).
- [68] B. I. Abelev, et al., Identified particle production, azimuthal anisotropy, and interferometry measurements in Au+Au collisions at  $\sqrt{s_{NN}} = 9.2 - 200$  GeV, Phys. Rev. C 81 (2010) 024911. [doi:10.1103/PhysRevC.81.024911](https://arxiv.org/abs/10.1103/PhysRevC.81.024911).
- [69] J. Jia, S. Mohapatra, Disentangling flow and non-flow correlations via Bayesian unfolding of the event-by-event distributions of harmonic coefficients in ultrarelativistic heavy-ion collisions, Phys. Rev. C 88 (1) (2013) 014907. [arXiv:1304.1471](https://arxiv.org/abs/1304.1471), doi:[10.1103/PhysRevC.88.014907](https://doi.org/10.1103/PhysRevC.88.014907).
- [70] J. Jia, M. Zhou, A. Trzupek, Revealing long-range multiparticle collectivity in small collision systems via subevent cumulants, Phys. Rev. C96 (3) (2017) 034906. [arXiv:1701.03830](https://arxiv.org/abs/1701.03830), doi:[10.1103/PhysRevC.96.034906](https://doi.org/10.1103/PhysRevC.96.034906).
- [71] P. Huo, K. Gajdošová, J. Jia, Y. Zhou, Importance of non-flow in mixed-harmonic multiparticle correlations in small collision systems, Phys.

- Lett. B 777 (2018) 201–206. [arXiv:1710.07567](#), doi:10.1016/j.physletb.2017.12.035.
- [72] C. Zhang, J. Jia, J. Xu, Non-flow effects in three-particle mixed-harmonic azimuthal correlations in small collision systems, Phys. Lett. B792 (2019) 138–141. [arXiv:1812.03536](#), doi:10.1016/j.physletb.2019.03.035.
- [73] N. Magdy, O. Evdokimov, R. A. Lacey, A method to test the coupling strength of the linear and nonlinear contributions to higher-order flow harmonics via Event Shape Engineering, J. Phys. G 48 (2) (2020) 025101. [arXiv:2002.04583](#), doi:10.1088/1361-6471/abcb59.
- [74] C. Zhang, A. Behera, S. Bhatta, J. Jia, Non-flow effects in correlation between harmonic flow and transverse momentum in nuclear collisions (2 2021). [arXiv:2102.05200](#).
- [75] N. Magdy, Measuring differential flow angle fluctuations in relativistic nuclear collisions, Phys. Rev. C 106 (4) (2022) 044911. [arXiv:2207.04530](#), doi:10.1103/PhysRevC.106.044911.
- [76] P. Bozek, R. Samanta, Higher order cumulants of transverse momentum and harmonic flow in relativistic heavy ion collisions, Phys. Rev. C 104 (1) (2021) 014905. [arXiv:2103.15338](#), doi:10.1103/PhysRevC.104.014905.
- [77] B. B. Abelev, et al., Event-by-event mean  $p_T$  fluctuations in pp and Pb-Pb collisions at the LHC, Eur. Phys. J. C 74 (10) (2014) 3077. [arXiv:1407.5530](#), doi:10.1140/epjc/s10052-014-3077-y.
- [78] B. B. Abelev, et al., Event-by-event mean  $p_T$  fluctuations in pp and Pb-Pb collisions at the LHC, Eur. Phys. J. C 74 (10) (2014) 3077. [arXiv:1407.5530](#), doi:10.1140/epjc/s10052-014-3077-y.
- [79] G. Aad, et al., Measurement of flow harmonics correlations with mean transverse momentum in lead-lead and proton-lead collisions at  $\sqrt{s_{NN}} = 5.02$  TeV with the ATLAS detector, Eur. Phys. J. C 79 (12) (2019) 985. [arXiv:1907.05176](#), doi:10.1140/epjc/s10052-019-7489-6.
- [80] P. Bozek, H. Mehrabpour, Correlation coefficient between harmonic flow and transverse momentum in heavy-ion collisions, Phys. Rev. C 101 (6) (2020) 064902. [arXiv:2002.08832](#), doi:10.1103/PhysRevC.101.064902.
- [81] B. Schenke, C. Shen, P. Tribedy, Multi-particle and charge-dependent azimuthal correlations in heavy-ion collisions at the Relativistic Heavy-Ion Collider, Phys. Rev. C 99 (4) (2019) 044908. [arXiv:1901.04378](#), doi:10.1103/PhysRevC.99.044908.
- [82] P. Alba, V. Mantovani Sarti, J. Noronha, J. Noronha-Hostler, P. Parotto, I. P. Vazquez, C. Ratti, Effect of the QCD equation of state and strange hadronic resonances on multiparticle correlations in heavy ion collisions (2017). [arXiv:1711.05207](#).
- [83] S. Acharya, et al., Characterizing the initial conditions of heavy-ion collisions at the LHC with mean transverse momentum and anisotropic flow correlations, Phys. Lett. B 834 (2022) 137393. [arXiv:2111.06106](#), doi:10.1016/j.physletb.2022.137393.
- [84] N. Magdy, R. A. Lacey, Model investigations of the correlation between the mean transverse momentum and anisotropic flow in shape-engineered events, Phys. Lett. B 821 (2021) 136625. [arXiv:2105.04879](#), doi:10.1016/j.physletb.2021.136625.
- [85] N. Magdy, P. Parfenov, A. Tarantenko, I. Karpenko, R. A. Lacey, Model study of the energy dependence of the correlation between anisotropic flow and the mean transverse momentum in Au+Au collisions, Phys. Rev. C 105 (4) (2022) 044901. [arXiv:2111.07406](#), doi:10.1103/PhysRevC.105.044901.
- [86] M. Abdallah, et al., Collision-System and Beam-Energy Dependence of Anisotropic Flow Fluctuations, Phys. Rev. Lett. 129 (25) (2022) 252301. [arXiv:2201.10365](#), doi:10.1103/PhysRevLett.129.252301.
- [87] B. Aboona, et al., Beam energy dependence of the linear and mode-coupled flow harmonics in Au+Au collisions, Phys. Lett. B 839 (2023) 137755. [arXiv:2211.11637](#), doi:10.1016/j.physletb.2023.137755.